














Characterization in the extreme ultraviolet (XUV) domain of microchannel plate based device using synchrotron radiation

Zeinab Ebrahimpour,^{1,a)}  Awad E. A. Mohamed,^{2,3}  Gabriele Bonano,⁴  Marco Cauero,⁵ 
Marcello Coreno,^{1,2}  Sultan B. Dabagov,¹  Massimo Ferrario,¹  Mikhail I. Mazuritskiy,⁶  Javad Rezvani,^{1,3} 
Francesco Stellato,⁷  Nicola Zema,⁸  Fabio Zuccaro,²  and Augusto Marcelli^{1,2,9} 

AFFILIATIONS

¹INFN-Laboratori Nazionali di Frascati, Via E. Fermi 54, 00044 Frascati, Italy

²CNR—Istituto Struttura della Materia and Elettra-Sincrotrone Trieste, Basovizza Area Science Park, 34149 Trieste, Italy

³Physics Division, School of Science and Technology, Università di Camerino, Via Madonna delle Carceri 9, Camerino, MC, Italy

⁴Department of Physics, Informatics, and Mathematics, University of Modena and Reggio Emilia, Via G. Campi 213/a, 41125 Modena, Italy

⁵Department of Engineering and Architecture, University of Trieste, 34127 Trieste, Italy

⁶Physics Department, Southern Federal University, 344090 Rostov-on-Don, Russia

⁷Physics Department, University of Rome Tor Vergata, and INFN—Sezione di Roma Tor Vergata, Via della Ricerca Scientifica 1, 00133 Roma, Italy

⁸ISM-CNR, Istituto Struttura della Materia, Via del Fosso del Cavaliere 100, 00133 Rome, Italy

⁹International Centre for Material Science Superstripes, RICMASS, Via dei Sabelli 119A, 00185 Rome, Italy

^{a)} Author to whom correspondence should be addressed: zeinab.ebrahimpour@lnf.infn.it

ABSTRACT

Innovative, low-loss, and compact optical systems are essential to meet the experimental requirements of emerging novel radiation sources. The microchannel plate (MCP), a metamaterial-based optical device, shows promising potential for shaping, condensing, and focusing soft x-ray radiation at synchrotron radiation (SR) facilities. This study highlights the impact of MCP optical devices on SR beam condensing capability and their sensitivity to the degree of coherence by investigating the profile of transmitted beams through single and double MCP optical devices. Transmitted diffraction patterns of soft x-ray SR radiation change with energy and radiation modes. At 92 eV, the double MCP-based device affects the beam divergence and degree of coherence more than the single MCP. Moreover, the double MCP device shows potential as a condensing optics at shorter wavelengths, i.e., 480 eV. Experiments were performed at the available end-station of the Circular Polarization beamline at the Elettra synchrotron facility in Trieste, using a high-vacuum chamber with a hexapod system, providing the precise movement necessary to align these diffractive optics. The findings contribute to the development of innovative optical systems for SR and free-electron laser beamlines, paving the way for advanced experiments in spectroscopy, microscopy, and imaging in a wide energy range.

I. INTRODUCTION

The availability of novel synchrotron radiation (SR) and free-electron laser (FEL) sources, which deliver highly brilliant, wavelength-tunable, coherent, and ultrashort photon pulses, is triggering new fundamental and technological applications.¹⁻⁴

New high-gradient acceleration techniques, such as particle- and laser-driven plasma acceleration, are under development to fulfill the demand for more compact, efficient, and high-quality radiation facilities.⁵⁻⁹ However, these new sources require innovative, low-loss, and compact optical systems to match

experimental requirements for power, polarization, coherence, etc., which are sometimes significantly limited by conventional optical systems. New optical components capable of condensing, monochromatizing, focusing, and/or filtering radiation, as well as manipulating its polarization and phase are under development, in particular, for highly coherent non-thermal sources.

In this regard, metamaterial-based optical devices represent a unique opportunity because of their flexibility, improved space integration, and compact design.^{10–13} In fact, such optics can control and tune radiation properties, such as phase, amplitude, and polarization more effectively than existing optics. The tunability of these optics is made possible by changing shape, dimension, position, symmetry, and relative orientation. An example of such optics is a microchannel plate (MCP): thin lead silicate glass plate, flat or bent, in the transverse section of which consisting of a periodic array of cylindrical or rectangular microchannels. Because of their strong interaction with charged particles and energetic photons, flexibility, and low cost, MCPs have been used in instruments for material science, astronomy, e-beam fusion, nuclear science, and other applications.^{14–21}

The physics of the radiation passage through MCPs is similar to polycapillary optics, i.e., based on that of conventional capillary guides.²² The transportation of radiation is governed by the interplay of grazing incidence and total reflection phenomena occurring at the surface, but we need to consider the transmission of the radiation as wave propagation in the frame of an electro-dynamical theoretical approach.^{23,24} MCP properties, coupled with their high flexibility and compactness, make these optics and their devices useful in a wide range of research for different purposes, such as filtering, condensing, and focusing, and for applications, such as x-ray fluorescence and x-ray scanning microscopy. Moreover, with their high transmission efficiency, MCPs could be successfully applied as diffraction gratings in a wide energy range.

MCPs have already been used in low-power instruments, leading to technological breakthroughs and applications using conventional sources.^{18–20} Using SR sources, the characterization of flat and bent MCPs already pointed out promising possibilities to shape, condense, and focus soft x-ray radiation at SR facilities.^{21,23–25} More recent theoretical analyses and preliminary experiments have demonstrated that the configuration of a couple of MCPs properly oriented and aligned offers new condensing and beam profiling capabilities.²⁴ The theoretical model based on the field transmission mode of radiation demonstrates that when coupling two MCPs, the electromagnetic field incident on the second MCP is the diffracted component of the coherent and monochromatic radiation exiting from the first MCP.

New coherent sources are also leading to spectacular advancements in material science, engineering, and medicine thanks to new techniques, such as partially coherent diffraction and x-ray phase contrast imaging.²⁶ The Young’s slits approach, which considers a fixed-size source and pinholes set at different distances to investigate the optical field, is the conventional approach for evaluating the spatial coherence of a radiation source.^{27–31} It has been reported that the source’s coherence properties could be determined by probing the field with a set of slits of fixed size and separation and modifying the source dimension by changing the aperture of the slit.³² The double slit experiment provides a clear

distinction between classical and wave optical behavior. In this regard, multi-slit experiments, such as those made possible by MCP systems, have the potential to provide fundamental information for investigating quantum and higher-order interference theories.^{33,34}

In the following, we will describe the optical layout and, in particular, the high-vacuum chamber available at the Circular Polarization (CiPo) beamline at ELETTRA.³⁵ Preliminary characterizations of a single and a couple of MCPs will be presented in Sec. III. The experiments are based on the collection of 2D diffraction patterns and profiles that offer unique information regarding the change of the spatial coherence of the source and beam divergence. In Sec. V, we will present the upgrades in progress to this experimental end-station. The new optical layout is made by two micro-manipulators, i.e., two hexapods able to align different optics with six degrees of freedom.

II. EXPERIMENTAL END-STATION

A. The beamline at Elettra

The CiPo beamline at the Elettra Synchrotron Trieste delivers a radiation beam with variable polarization in a wide range of photon energies ranging from 5 to 900 eV. The radiation is emitted by an Electromagnetic Elliptical Wiggler (EEW) that can be operated both in undulator and wiggler modes. EEW radiation is dispersed alternatively by two collinear monochromators: a normal incidence monochromator (NIM) and a spherical grating monochromator (SGM) that share entrance and exit slits as well as pre- and post-focusing optics, keeping the position of the focus on the sample fixed. NIM configuration covers the UV–VUV energy range (5–40 eV), and SGM mode provides the soft x-ray domain (40–900 eV). The CiPo beamline allows several experimental activities thanks to the availability of a broad photon energy spectrum together with the polarization options.^{36,37} Beamline’s detailed description and characteristics, together with technical information, are available on the beamline webpage (<https://www.elettra.eu/elettra-beamlines/cipo.html>).

B. Experimental high-vacuum chamber

An overview of the experimental setup is shown in Fig. 1. The main component is a vacuum chamber that can work in the high-vacuum (HV) regime (10^{-5} Pa). The photon beam in the energy range of 90–500 eV provided by the SGM monochromator reaches the experimental chamber where different experiments, detailed below, can be carried out. To separate the ultrahigh vacuum of the beamline from the HV of the experimental chamber, a window made by a thin SiN film enables the transmission of XUV radiation down to 100 eV. A turbopump-based differential pumping system is also available between the final refocusing mirror and the experimental end-station. Its use depends on the spot-size requirement of the experiment and the operating distances of the end-station. The latter solution has been used to carry out the experiments described in Sec. IV.

Inside the HV chamber, a remote-control HV manipulator with six degrees of freedom, high precision, and large travel ranges is available. The HV hexapod system is characterized by high

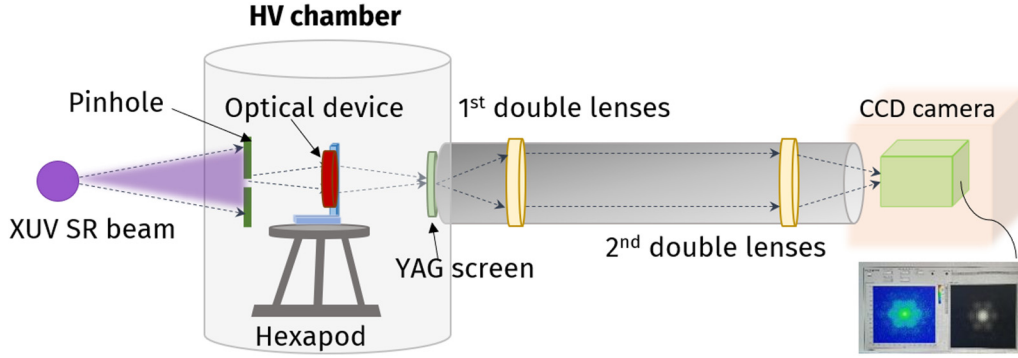


FIG. 1. A schematic side view of the high-vacuum (HV) experimental chamber available as end-station at the CiPo beamline; the SR radiation is coming from the left. The HV vacuum chamber hosts a six-axis manipulator and the detection system (out of scale on the right side of the graph). The optical device is an assembly of two flat MCPs.

precision motions, six degrees of freedom, and large translational and rotational travel ranges: ± 25 mm (X, Z), ± 6.25 mm (Y), and $\pm 5^\circ$ (θ_X , θ_Y , θ_Z). The absolute position accuracy has been measured at $10\ \mu\text{m}$ for linear and $50\ \mu\text{rad}$ for angular rotations, with a repeatability of $100\ \text{nm}$ and $10\ \mu\text{rad}$, respectively. This sample positioning offers a bidirectional repeatability of $\pm 0.5\ \mu\text{m}$ (X, Y, Z) and $\pm 20\ \mu\text{rad}$ (θ_X , θ_Y , θ_Z) at the minimum operating pressure of 10^{-5} Pa. The interferometric tests of this manipulator revealed an average static stability of up to $20\ \text{nm}$ over 1 min, offering a complete investigation of any optical component with a maximum weight of 1 kg.

C. Optical detection system

The optical layout inside the HV chamber is illustrated in Fig. 1. This layout defines the transmission properties, the angular distribution, and patterns of compact optical devices in this energy range. The detection system can collect all radiation transmitted by optics under test, such as MCP samples. A pinhole placed before the optics allows one to tune radiation properties, such as divergence and transverse coherence of the incoming radiation. A circular fluorescent YAG screen, beam collimating lenses, and a 2D detector constitute the detection system. The 25 mm-diameter YAG screen, which is placed downstream, transforms the diffracted distribution into a pattern at visible wavelengths through the scintillation effect. The resulting transmitted pattern in the visible wavelength range is collected by the 2D detector through two pairs of double lenses. The 2D detector is the sCMOS digital camera (Basler Ace aca2040-35 gm—Area Scan Camera); its resolution, 1 pixel = $3.5 \times 3.5\ \mu\text{m}^2$, has been evaluated by the analysis of the image of a $100\ \mu\text{m}$ -wide filament. The distance between the 2D detector and the optical components mounted on the second HV manipulator can be tuned in the range of 10–120 mm.

Using the station installed at CiPo, we could characterize both flat and bent MCP optics, detectors, and devices as reported in our previous works.^{23–25} We take advantage of the SR characteristics to collect specific and accurate spectra that require (i) a low divergent and highly brilliant intense radiation source, where the brilliance is

defined as the photon flux normalized to the solid angle and to the source area (photons/s/0.1%/mrad²/mm²) and (ii) a monochromatic coherent radiation and a high energy resolution in the energy range of 90–500 eV.

III. MATERIALS AND METHOD

The double microchannel plate (MCP) device we characterized is made by a couple of flat MCPs assembled and aligned parallel with micrometer-scale precision. As illustrated in Fig. 2, the primary radiation propagates along the z axis and passes through two coaxial polycapillary plates mechanically assembled in a rigid frame. Radiation is transmitted through the hollow microchannels of the MCP system and collected by a YAG screen positioned at the XY plane. In Fig. 2, the distance “d1” between the parallel plates MCP-1 and MCP-2 is $50\ \mu\text{m}$, while the YAG screen is situated in the distance represented by “d” away from the device. The MCP device³⁸ is made of silicon-lead glass with a mass concentration of $0.7\text{PbO} + 0.3\text{SiO}_2$. It comprises 10^4 – 10^7 regularly spaced and arranged hollow microchannels within a hexagonal symmetry in the transverse cross section, with an inner diameter of $10\ \mu\text{m}$ and a pitch of $12\ \mu\text{m}$ between the channels. The longitudinal cross section of the MCPs reveals a long channel structure with a length/diameter ratio of ~ 120 .

We were able to modify the angular orientation of this MCP device with high precision and accuracy using the six-stage micromanipulator. The layout-1 is shown in Fig. 2(a), where the primary beam propagates in the central area (along the axis) of the coaxially aligned MCP device. In this layout, MCP-1 is not illuminated and does not contribute to the process since the radiation is going through its wide central circular hole ($\sim 3\ \text{mm}$). The measurements of the radiation propagating inside both plates [Fig. 2(b)] were performed by shifting the device by about 2 mm from the center in the xy plane.

IV. RESULTS AND DISCUSSION

In this section, we present summarized results of the characterization of the MCP devices demonstrating the efficient

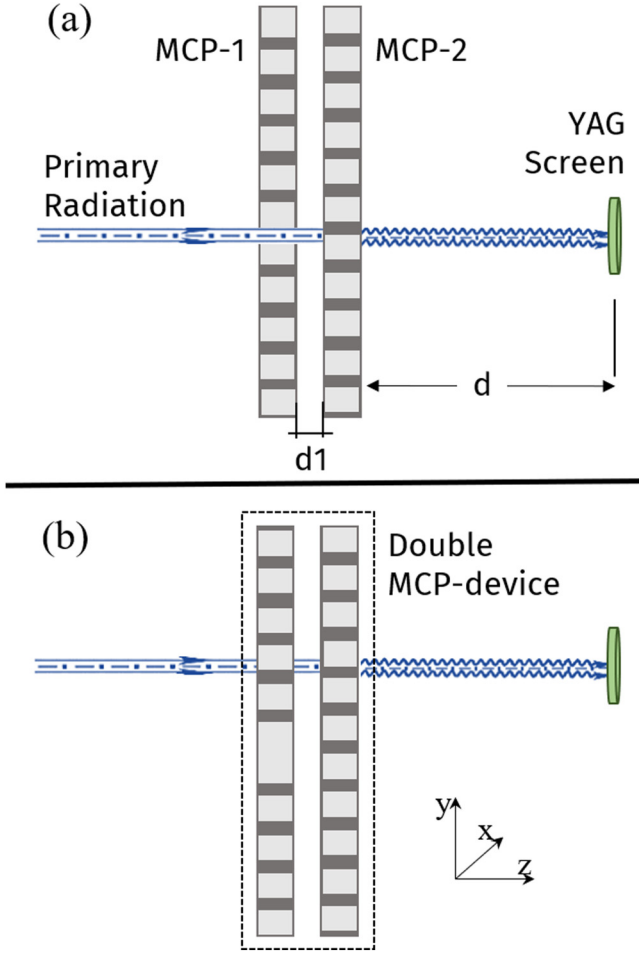


FIG. 2. The MCP device is made by two flat parallel coaxial MCPs: (a) layout-1 for transmission of radiation only by the MCP-2 and (b) layout-2 for transmission of radiation by both MCPs.

behavior of the couple of aligned MCPs as well as of the experimental end-station hosted at the CiPo beamline. The single and the couple of flat MCPs were tested at various positions of the detector (Fig. 3) and with various combinations of entrance and exit slits ($300 \times 300 \mu\text{m}^2$, $100 \times 100 \mu\text{m}^2$, and $50 \times 50 \mu\text{m}^2$) (Fig. 4). We compare the diffraction patterns produced by the devices made by two flat MCPs at normal incidence and at two different primary radiation energies: 92 and 480 eV selecting both wiggler and undulator modes (Fig. 5). The angular distribution of the beam (energy resolution) defined by entrance and exit slit sizes at 92 eV was 0.12, 0.24, and 0.72 eV and at 480 eV was 0.52, 1.04, and 3.04 eV for 50×50 , 100×100 , and $300 \times 300 \mu\text{m}^2$ slit openings, respectively. For these experiments, pinholes with diameters of 30 and $100 \mu\text{m}$ were set in the HV chamber before the optics to modify the beam size. All intensities recorded by the camera have been normalized to the photodiode current. The images presented in the figures are the average of a collection of 10–50 images.

A. Divergence of the beam radiation

Figures 3(a) and 3(b) show (as representative of the results) the radiation at 92 eV transmitted from a single MCP and a couple of MCPs located at various distances from the YAG screen. The MCP device diffracts the SR beam in an undulator mode with a defined beam size through the $300 \times 300 \mu\text{m}^2$ slit and the $30 \mu\text{m}$ -sized pinhole located before the device. The images are formed by 150×150 pixels, corresponding to $\sim 525 \times 525 \mu\text{m}^2$ (considering the size of each pixel to be $3.5 \mu\text{m}$). Precise alignment and setup optimization for each data acquisition determine the contrast of these images. The diffraction patterns exhibit a hexagonal symmetry similar to that of the MCPs for both optics. However, the patterns generated by the couple of MCPs have a finer structure.

We estimate the beam divergence using the distance-dependent transmission measurements. We measured the beam waist parameter (w) obtained from the Gaussian fit of the horizontal profile of the pattern at two different distances (d) noted by 1 and 2 and the relation $\theta = \frac{w_2 - w_1}{d_2 - d_1}$. The radiation divergence in free space, without the presence of an MCP device, was calculated to be 0.889 ± 0.064 mrad. After passing through a single MCP, the θ value was measured to be 1.392 ± 0.064 mrad. Similarly, for the couple of MCP devices, it was determined to be 1.437 ± 0.064 mrad. These values indicate that the MCP device increases the beam divergence, and the couple of MCPs exhibit a larger divergence. A detailed analysis of the results points out that the divergence of the transmitted beam is influenced by the primary SR beam parameters, spot size, and the characteristics of the optical device. For example, using a single MCP device with the source in the wiggler mode, while keeping constant the other parameters, the divergence was measured to be 1.214 ± 0.064 mrad. Despite the increased divergence, it is worth noting that the higher concentration of beam intensity in the central peaks suggests the potential for further optimization of the device as condensing optics.

B. Coherence evaluation

In Figs. 4(a)–4(f), we compare diffraction patterns and beam intensity profiles of the transmitted SR beam at 92 eV in the undulator regime beyond both the single MCP and couple of MCP devices. The measurements are performed for different apertures of the entrance and exit slits, while the pinhole defining the beam size is set to $100 \mu\text{m}$. As we can see in the figure, more intense peaks are visible in the diffraction patterns generated by the couple of MCP devices [Figs. 4(d)–4(f)]. Moreover, these patterns are more complex than those generated by the single MCP [Figs. 4(a)–4(c)]. This is due to the fact that the radiation hitting the 2nd MCP is the diffracted radiation by the 1st MCP. Therefore, both the distance and the relative angular position of the 2nd MCP respect to the 1st one define the image generated by this MCP-based optical device. Below, we will evaluate the coherence of the transmitted radiation using the patterns shown in Fig. 4.

The degree of coherence is a concept defined as the normalized mutual coherence function, where the incoming radiation is represented by a monochromatic plane wave with a Gaussian distribution of the intensity in the transverse cross section. The spatial coherence can be described by the first-order mutual correlation

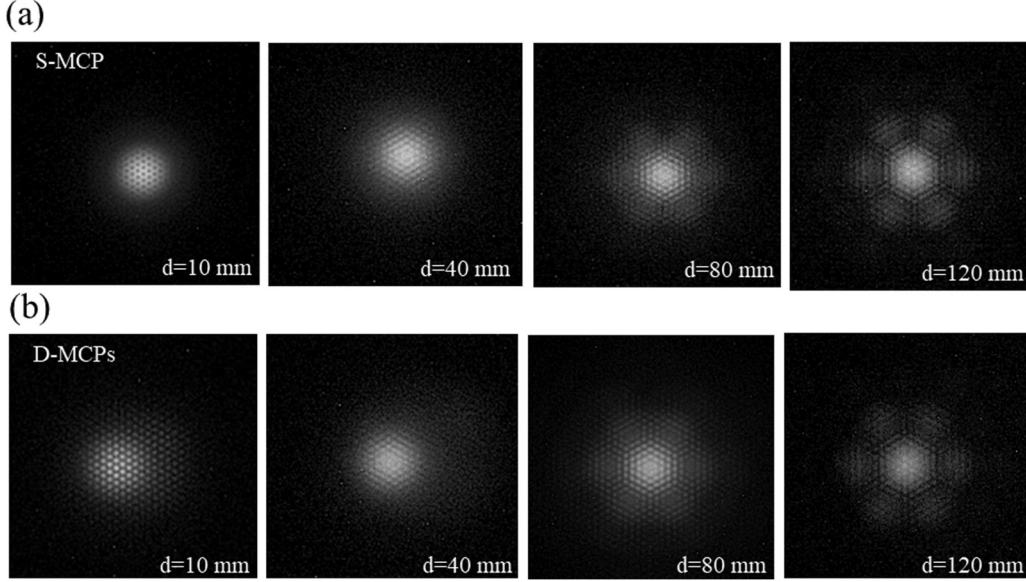


FIG. 3. The diffraction patterns produced by (a) a single flat MCP and (b) two flat MCPs coupled together and placed at different distances, d , from the detector (YAG screen). The images (150×150 pixels) have been collected by the camera at the photon energy of 92 eV. The source was set in the undulator mode and slits opened to $300 \times 300 \mu\text{m}^2$. A $30 \mu\text{m}$ pinhole was located before the optics.

function of the electric field,³⁹ defined as

$$\gamma^{(1)}(r_1, r_2, \tau) = \frac{\langle E^*(r_1, t)E(r_2, t + \tau) \rangle}{\langle \sqrt{I(r_1, t)I(r_2, t)} \rangle}, \quad (1)$$

where $E(r_1, t)$ and $E(r_2, t + \tau)$ are the electric fields at the defined positions and time r_1, t and $r_2, t + \tau$, respectively, $I(r, t)$ is the intensity at the position r and time t , $\langle \dots \rangle$ is the ensemble average, while $*$ refers to the complex conjugate of the parameter. By considering the same incident intensity illuminating different parts of the optical device, $\gamma^{(1)}$ can be defined as the visibility parameter,

$$V = \gamma^{(1)} = \frac{I_{\max} - I_{\min}}{I_{\max} + I_{\min}}, \quad (2)$$

where I_{\max} and I_{\min} are the maximum and minimum intensities of the interference fringes.^{26–32} The visibility of the interference patterns provides a measure of the coherence between pairs of points (I_{\max} and I_{\min}) on the profile of the diffraction pattern. The visibility (V) of the patterns for the first order peaks can be calculated using the horizontal profile of each pattern. By increasing the size of the slits that limits the source dimension, the visibility of the patterns decreases from 0.77 to 0.68 and from 0.74 to 0.64 for the single MCP and a couple of MCP devices, respectively.

A similar behavior was observed for the second and third orders of visibility parameters of the patterns. The visibility for the MCP-based device is lower than the single MCP, a condition that may be associated with the second-diffraction process occurring in

the device. It suggests that the device affects the coherence of the transmitted beam. A comprehensive evaluation of the coherence characteristics of transmitted SR beams through MCP devices is in progress.

In Figs. 5(a)–5(c), the transmitted beam profiles of a couple of MCPs are compared for the undulator and wiggler modes at the photon energies of 92 and 480 eV keeping a constant slit aperture ($300 \times 300 \mu\text{m}^2$) and a pinhole size ($100 \mu\text{m}$). At 92 eV photon energy, the transmitted beam has hexagonally symmetric diffraction patterns, while at 480 eV, it displays a gaussian distribution.

The peak analysis of the horizontal profile of the diffraction patterns reveals that in the undulator regime, the intensity is concentrated in the central and first order peaks with up to nine peaks clearly detectable. While in the wiggler mode, the intensity is distributed over only five peaks. The different peak numbers may also be connected with the different degrees of spatial coherence of the incoming beam between the undulator and wiggler regime. In both conditions, the distance between peaks is 44 ± 1 pixel. The full width at half maximum (FWHM) of the central peak and of the full beam are 27 and 94 pixels in the undulator regime, as well as 24 and 90 pixels in the wiggler mode. Instead, the transmitted SR beam profile at 480 eV displayed in Fig. 6(c) is a simply condensed gaussian distribution with a FWHM of 27 pixels, corresponding after the calibration to $95 \mu\text{m}$. Moreover, using the distance-dependent transmission measurements, the method presented in Sec. IV A, we obtained a very small beam divergence of 0.203 mrad. The results point out the use of the MCP-based device as an effective condensing optics for an SR beam in this energy range.

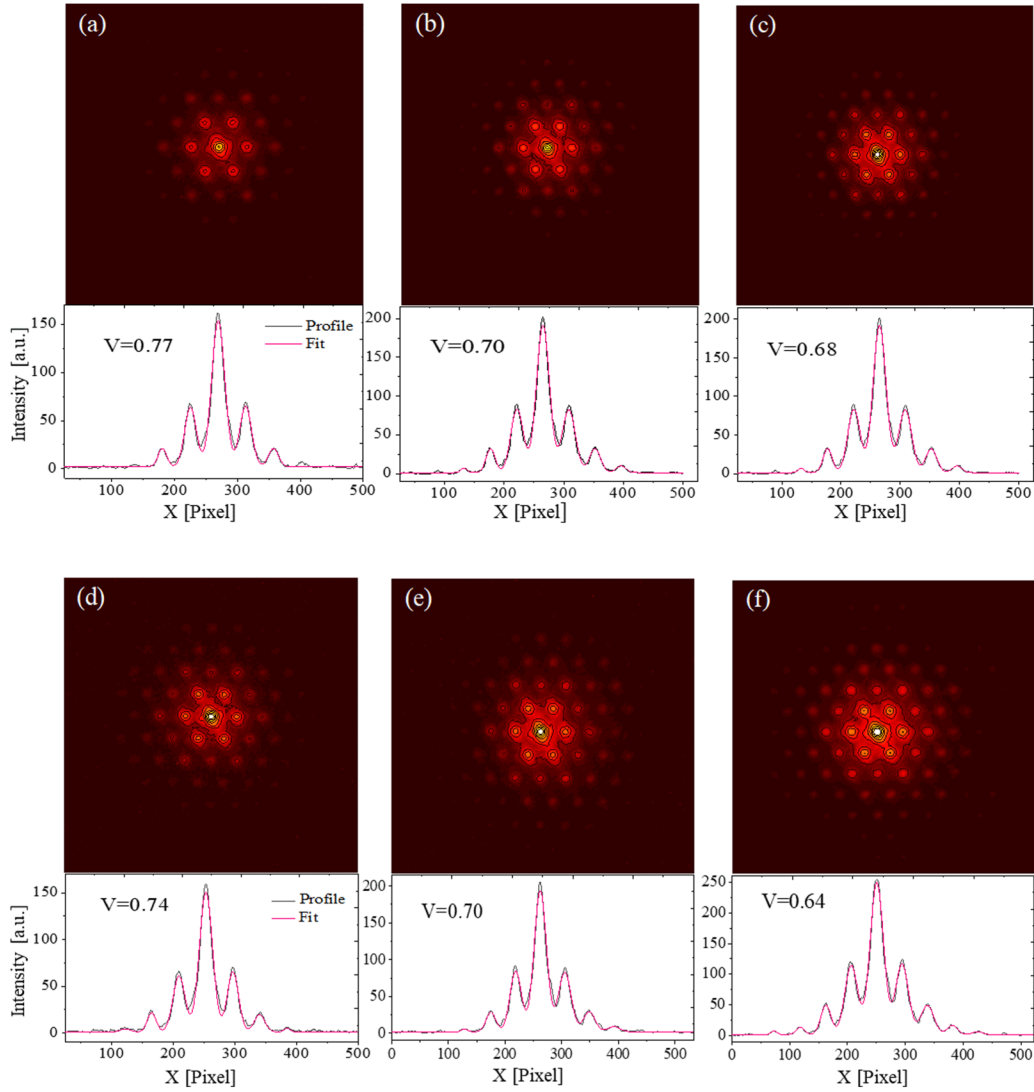


FIG. 4. In each panel, we show the diffraction pattern and the central horizontal profile of the beam transmitted from (a)–(c) the single MCP and (d)–(f) the two assembled MCPs. The radiation at 92 eV was emitted by the source set in an undulator mode. The entrance and exit slits are (a) and (d) $50 \times 50 \mu\text{m}^2$, (b) and (e) $100 \times 100 \mu\text{m}^2$, and (c) and (f) $300 \times 300 \mu\text{m}^2$, while the pinhole ($100 \mu\text{m}^2$) and the distance (120 mm) between the device and the detector are the same for all the patterns. The Vs in the insets indicate the visibility parameter.

V. EXPERIMENTAL UPGRADES AND OUTLOOK

The end-station installed at the CiPo beamline at the Elettra synchrotron facility in Trieste is undergoing upgrades with an additional hexapod to enhance its capabilities for testing and characterizing of different optical devices: microchannel plates (MCPs), capillary optics, zone plates, filters, condensers, detectors, etc. A second hexapod is currently being installed, enabling the simultaneous alignment with micrometer positioning of a second optical element. The new hexapod is more compact and can also operate in the HV regime. It allows accurate motions with six degrees of

freedom. This new hexapod is more compact and operates at pressures within the range of 10^{-4} Pa. It offers high precision motion with six degrees of freedom. The translational range for all axes of the second hexapod is defined as ± 50 mm (X, Y, Z), while the rotational range is $\pm 5^\circ$ (θ_X , θ_Y , θ_Z). This configuration allows simultaneous motions of two optical elements, enabling users to precisely control the distance and orientation of both optics.

The utilization of two HV manipulators in this optical setup provides users with the ability to fully align and remotely control two optical elements with high accuracy. This capability proves extremely valuable for characterizing various compact optical

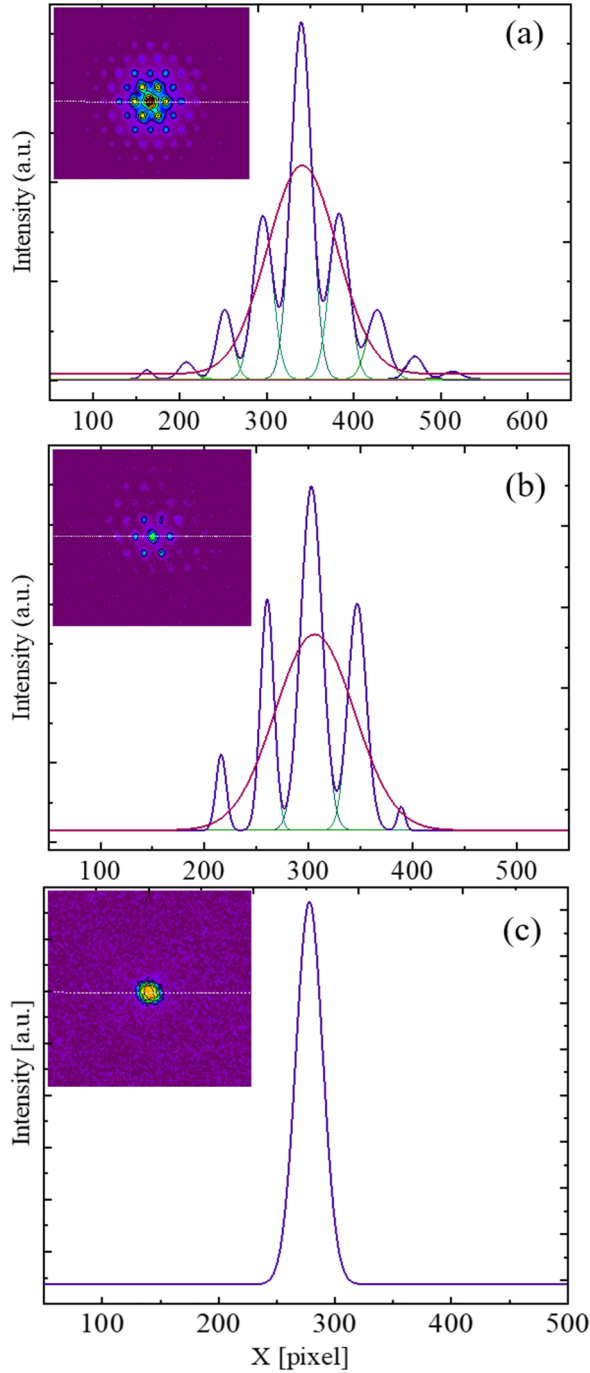


FIG. 5. The central horizontal profiles of the diffraction patterns (shown in the insets) produced by the couple of MCP devices for different incident beams: (a) $E_{ph} = 92$ eV in the undulator mode, (b) $E_{ph} = 92$ eV in the wiggler mode, and (c) $E_{ph} = 480$ eV in the wiggler mode. The slit aperture of $300 \times 300 \mu\text{m}^2$, the pinhole size of $100 \mu\text{m}$, and the distance between the device and the YAG screen $d = 120$ mm were fixed for all the patterns. The Gaussian total and peak analysis fits are represented by the curves in red and green, respectively.

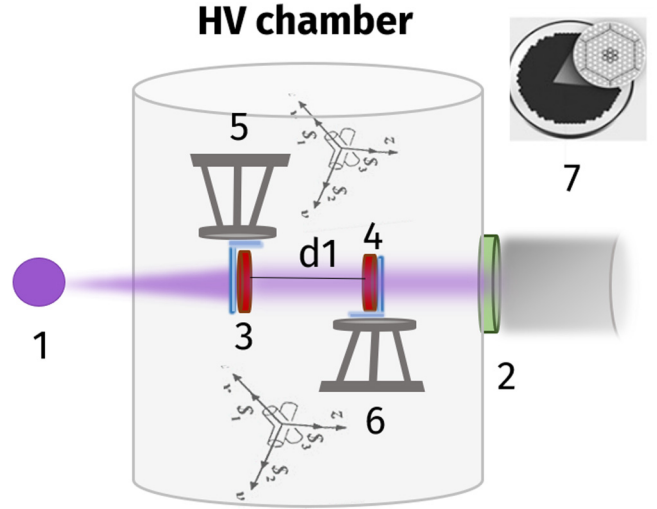


FIG. 6. Experimental layout using two MCPs (3) and (4) to be aligned in remote inside the HV chamber. The other components of the layout are the primary beam (1), the detector (2), and the two hexapods (5) and (6) designed for precision orientation of the MCPs. We can control the distance ($d1$) between the two MCPs and the symmetry of the structure of the MCPs (7).

systems in the transmission mode and offers the opportunity to test new microscopy and imaging setups with synchrotron radiation (SR) and free-electron laser (FEL) sources. Additionally, this setup facilitates the investigation of radiation propagation modes in glassy waveguides and the observation of interference between incident and reflected (fluorescence) waves, providing unique insights into wave propagation phenomena.

The optical layout of the CiPo end-station we described here is essential for conducting comprehensive studies on flat and bent MCPs, MCP-based devices, and other compact photonic systems. The results presented in Fig. 4, combined with recent theoretical simulations we carried out, indicate that both the distance and relative angular position between MCPs define pattern and profile characteristics generated by the incoming radiation traveling inside devices made by a couple of MCPs. In Fig. 6, a possible experimental configuration utilizing the upgraded end-station is outlined. In this figure, the distance ($d1$) between the two MCPs and their orientation can be defined with high accuracy and repeatability.

VI. CONCLUSIONS

The availability of novel and powerful synchrotron radiation and free-electron laser sources is triggering the demand for innovative, compact, and low-loss optical systems that can preserve the coherence degree of the emitted radiation while offering high tunability in terms of energy and polarization. Among the various diffractive optics devices, microchannel plates (MCPs) have shown great potential in a wide range of applications for both radiation and particles.

This contribution compares the results of transmitted radiation through a single MCP and a pair of flat MCP optical devices. The experiments performed at the CiPo beamline at Elettra show the unique characteristics of the transmitted radiation through these meta-lenses that can be effectively tuned by the characteristics of the primary beam combined with the optics characteristics. Moreover, we show that a preliminary evaluation of the coherence is possible from the analysis of the diffraction patterns of MCPs, and multi-slit experiments can certainly be used to provide fundamental insights into quantum and higher-order interference theories, as well as to test quantum optics through the analysis of coherence phenomena. The ongoing experimental upgrades of the optical setup available at the CiPo beamline will play a great role in the characterization of new compact optical devices and diffractive optics. These studies will contribute to enhancing our understanding of wave propagation phenomena, the optimization of optical systems for third- and fourth-generation radiation sources, and the design of new optical layouts for spectroscopy, imaging, and microscopy techniques.

ACKNOWLEDGMENTS

The authors would like to acknowledge the support of the European Union Horizon 2020 research and innovation program [Grant Agreement No. 653782 (EuPRAXIA)]. The authors acknowledge Elettra Sincrotrone Trieste for providing access to its synchrotron radiation facilities and for financial support under the SUI internal project. This research has benefited from the results of the experiments performed at Elettra within Proposal No. 20215699. Awad E. A. Mohamed would like to acknowledge the support of the TRIL Program of the Abdus Salam International Centre for Theoretical Physics (ICTP).

AUTHOR DECLARATIONS

Conflict of Interest

The authors have no conflicts to disclose.

Author Contributions

Zeinab Ebrahimpour: Conceptualization (equal); Data curation (equal); Formal analysis (equal); Investigation (equal); Methodology (equal); Software (equal); Visualization (equal); Writing – original draft (equal); Writing – review & editing (equal). **Awad E. A. Mohamed:** Data curation (equal); Formal analysis (equal). **Gabriele Bonano:** Data curation (equal). **Marco Cautero:** Software (equal). **Marcello Coreno:** Data curation (equal); Resources (equal). **Sultan B. Dabagov:** Investigation (equal); Writing – review & editing (equal). **Massimo Ferrario:** Funding acquisition (equal). **Mikhail I. Mazuritskiy:** Conceptualization (equal); Formal analysis (supporting); Resources (equal); Visualization (supporting); Writing – review & editing (equal). **Javad Rezvani:** Data curation (equal); Software (equal); Writing – review & editing (equal). **Francesco Stellato:** Funding acquisition (equal); Writing – review & editing (supporting). **Nicola Zema:** Data curation (supporting); Resources (equal); Writing – review & editing (equal). **Fabio Zuccaro:** Data curation (supporting). **Augusto Marcelli:** Conceptualization (equal); Data

curation (equal); Funding acquisition (equal); Investigation (equal); Methodology (equal); Supervision (lead); Writing – review & editing (lead).

DATA AVAILABILITY

The data that support the findings of this study are available from the corresponding author upon reasonable request.

REFERENCES

- ¹I. Matsuda and Y. Kubota, “Recent progress in spectroscopies using soft x-ray free-electron lasers,” *Chem. Lett.* **50**, 1336–1344 (2021).
- ²J. Zhong, H. Zhang, X. Sun, and S. T. Lee, “Synchrotron soft x-ray absorption spectroscopy study of carbon and silicon nanostructures for energy applications,” *Adv. Mater.* **26**, 7786–7806 (2014).
- ³B. A. Collins and E. Gann, “Resonant soft x-ray scattering in polymer science,” *J. Polym. Sci.* **60**, 1199–1243 (2022).
- ⁴Z. Ebrahimpour, M. Coreno, L. Giannessi, M. Ferrario, A. Marcelli, F. Nguyen, S. J. Rezvani, F. Stellato *et al.*, “Progress and perspectives of spectroscopic studies at carbon K-edge using novel soft X-ray pulsed sources,” *Condens. Matter* **7**, 72 (2022).
- ⁵M. Ferrario, D. Alesini, M. P. Anania, M. Artioli, A. Bacci, S. Bartocci, R. Bedogni, M. Bellaveglia *et al.*, “EuPRAXIA@SPARC_LAB design study towards a compact FEL facility at LNF,” *Nucl. Instrum. Methods Phys. Res. Sect. A* **909**, 134–138 (2018).
- ⁶R. Pompili, E. Chiadroni, A. Cianchi, M. Ferrario, A. Gallo, V. Shpakov, and F. Villa, “From SPARC_LAB to EuPRAXIA@SPARC_LAB,” *Instruments* **3**, 45 (2019).
- ⁷V. Petrillo, A. Bacci, E. Chiadroni, G. Dattoli, M. Ferrario, A. Giribono, A. Marocchino, A. Petralia *et al.*, “Free electron laser in the water window with plasma driven electron beams,” *Nucl. Instrum. Methods Phys. Res. Sect. A* **909**, 303–308 (2018).
- ⁸F. Villa, M. Coreno, Z. Ebrahimpour, L. Giannessi, A. Marcelli, M. Opromolla, V. Petrillo, and F. Stellato, “ARIA—A VUV beamline for EuPRAXIA@SPARC_LAB,” *Condens. Matter* **7**, 11 (2022).
- ⁹A. Balerna, M. Ferrario, and F. Stellato, “The INFN-LNF present and future accelerator-based light facilities,” *Eur. Phys. J. Plus* **138**(1), 37 (2023).
- ¹⁰N. S. Kumar, K. C. B. Naidu, P. Banerjee, T. A. Babu, and B. V. S. Reddy, “A review on metamaterials for device applications,” *Crystals* **11**(5), 518 (2021).
- ¹¹H. Liu, M. Zhao, Y. Gong, K. Li, C. Wang, Y. Wei, J. Wang, G. Liu, J. Yao, Y. Li *et al.*, “A high precision and multifunctional electro-optical conversion efficiency measurement system for metamaterial-based thermal emitters,” *Sensors* **22**(4), 1313 (2022).
- ¹²Y. Han, J. Lin, and Y. S. Lin, “Tunable metamaterial-based silicon waveguide,” *Opt. Lett.* **45**, 6619–6622 (2020).
- ¹³A. Alvarez-Fernandez, C. Cummins, M. Saba, U. Steiner, G. Fleury, V. Ponsinet, and S. Guldin, “Block copolymer directed metamaterials and metasurfaces for novel optical devices,” *Adv. Opt. Mater.* **9**(16), 2100175 (2021).
- ¹⁴J. Ladislav Wiza, “Microchannel plate detectors,” *Nucl. Instrum. Methods* **162**, 587–601 (1979).
- ¹⁵G. Vinelli, R. Ferragut, M. Giammarchi, G. Maero, M. Romé, and V. Toso, “Real-time monitoring of a positron beam using a microchannel plate in single-particle mode,” *J. Instrum.* **15**, P11030 (2020).
- ¹⁶A. S. Tremsin and J. V. Vallerga, “Unique capabilities and applications of microchannel plate (MCP) detectors with Medipix/Timepix readout,” *Radiat. Meas.* **130**, 106228 (2020).
- ¹⁷T. Cremer, B. W. Adams, M. Aviles, C. Ertley, M. R. Foley, A. V. Lyashenko, M. J. Minot, M. A. Popecki *et al.*, “Recent developments on next-generation microchannel plates for particle identification applications,” *Proc. SPIE* **11118**, 111180M (2019).
- ¹⁸J. De Keyser, K. Altwegg, A. Gibbons, F. Dhooghe, H. Balsiger, J. J. Berthelier, S. A. Fuselier, T. I. Gombosi *et al.*, “Position-dependent microchannel plate gain

- correction in Rosetta's ROSINA/DFMS mass spectrometer," *Int. J. Mass Spectrom.* **446**, 116232 (2019).
- ¹⁹Y. Yang, B. Zhu, Y. Gou, Z. Chen, X. Bai, J. Qin, Y. Bai, B. Liu *et al.*, "A sealed x-ray microchannel plate imager with CsI photocathode to improve quantitative precision of framing camera," *Nucl. Instrum. Methods Phys. Res. Sect. A* **1005**, 165404 (2021).
- ²⁰S. Diebold, "Proportional counters and microchannel plates," [arXiv:2210.10883](https://arxiv.org/abs/2210.10883) (2022).
- ²¹M. I. Mazuritskiy, A. M. Lerer, A. Marcelli, S. B. Dabagov, M. Coreno, A. D'Elia, and S. J. Rezvani, "Wave propagation and focusing of soft x-rays by spherical bent microchannel plates," *J. Synchrotron Radiat.* **28**, 383–391 (2021).
- ²²S. Dabagov and A. Dik, "Surface channeling of charged and neutral beams in capillary guides," *Quantum Beam Sci.* **6**, 8–20 (2022).
- ²³M. I. Mazuritskiy, S. B. Dabagov, A. Marcelli, K. Dziedzic-Kocurek, and A. M. Lerer, "X-ray radiation channeling in micro-channel plates: Spectroscopy with a synchrotron radiation beam," *Nucl. Instrum. Methods Phys. Res. Sect. B* **355**, 293–296 (2015).
- ²⁴M. I. Mazuritskiy, A. M. Lerer, A. Marcelli, and S. B. Dabagov, "Synchrotron radiation transmission by two coupled flat microchannel plates: New opportunities to control the focal spot characteristics," *J. Synchrotron Radiat.* **29**, 355–362 (2022).
- ²⁵M. I. Mazuritskiy, A. M. Lerer, S. B. Dabagov, and A. Marcelli, "Coherent x-ray fluorescent excitation inside MCP microchannels: Axial channeling and wave propagation," *J. Surf. Investig. X-Ray Synchrotron Neutron Tech.* **15**, 513–519 (2021).
- ²⁶K. A. Nugent, "Coherent methods in the x-ray sciences," *Adv. Phys.* **59**(1), 1–99 (2010).
- ²⁷D. Paterson, B. E. Allman, P. J. McMahon, J. Lin, N. Moldovan, K. A. Nugent, I. McNulty, C. T. Chantler *et al.*, "Spatial coherence measurement of x-ray undulator radiation," *Opt. Commun.* **195**(1-4), 79–84 (2001).
- ²⁸P. Skopintsev, A. Singer, J. Bach, L. Müller, B. Beyersdorff, S. Schleitner, O. Gorobtsov, A. Shabalin *et al.*, "Characterization of spatial coherence of synchrotron radiation with non-redundant arrays of apertures," *J. Synchrotron Radiat.* **21**, 722–728 (2014).
- ²⁹I. A. Vartanyants, A. Singer, A. P. Mancuso, O. M. Yefanov, A. Sakdinawat, Y. Liu, E. Bang, G. J. Williams *et al.*, "Coherence properties of individual femto-second pulses of an x-ray free-electron laser," *Phys. Rev. Lett.* **107**, 144801 (2011).
- ³⁰M. C. Marconi, J. L. A. Chilla, B. R. Benware, and J. J. Rocca, "Measurement of the spatial coherence buildup in a discharge pumped table-top soft x-ray laser," *Phys. Rev. Lett.* **79**, 2799–2802 (1997).
- ³¹B. Redding, M. A. Choma, and H. Cao, "Spatial coherence of random laser emission," *Opt. Lett.* **36**, 3404 (2011).
- ³²J. P. Sharpe and D. A. Collins, "Demonstration of optical spatial coherence using a variable width source," *Am. J. Phys.* **79**, 554–557 (2011).
- ³³A. Marcelli, M. I. Mazuritskiy, S. B. Dabagov, D. Hampai, A. M. Lerer, E. A. Izotova, A. D'Elia, S. Turchini *et al.*, "A new XUV optical end-station to characterize compact and flexible photonic devices using synchrotron radiation," *J. Instrum.* **13**, C03035 (2018).
- ³⁴H. Barnum, M. P. Müller, and C. Ududec, "Higher-order interference and single-system postulates characterizing quantum theory," *New J. Phys.* **16**, 123029 (2014).
- ³⁵U. Sinha, C. Couteau, T. Jennewein, R. Laflamme, and G. Weihs, "Ruling out multi-order interference in quantum mechanics," *Science* **329**, 418–421 (2010).
- ³⁶A. Derossi, F. Lama, M. Piacentini, T. Prosperi, and N. Zema, "High flux and high resolution beamline for elliptically polarized radiation in the vacuum ultraviolet and soft x-ray regions," *Rev. Sci. Instrum.* **66**, 1718–1720 (1995).
- ³⁷D. Desiderio, S. Difonzo, B. Diviacco, W. Jark, J. Krempasky, R. Krempaska, F. Lama, M. Luce, H. C. Mertins, M. Piacentini, T. Prosperi, S. Rinaldi, G. Soullie, F. Schäfers, F. Schmolle, L. Stichauer, S. Turchini, R. P. Walker, and N. Zema, "The elletra circular polarization beamline and electromagnetic elliptical wiggler insertion device," *Synchrotron Radiat. News* **12**, 34–38 (1999).
- ³⁸Vladikavkaz Technological Center "BASPIK"; see <http://www.baspik.com/eng/products/nauka/>.
- ³⁹J. W. Goodman, *Statistical Optics* (Wiley-Interscience, New York, 1985), Vol. 1, p. 567.